DOI: 10.1002/adfm.200600359

Efficient Organic Light-Emitting Diodes based on Sublimable Charged Iridium Phosphorescent Emitters**

By *Wai-Yeung Wong*,* *Gui-Jiang Zhou*, *Xiao-Ming Yu*, *Hoi-Sing Kwok*, and *Zhenyang Lin*

The synthesis and characterization of two new phosphorescent cationic iridium(III) cyclometalated diimine complexes with formula $[Ir(\mathbf{L})_2(N\text{-}N)]^+(PF_6^-)$ (**HL** = (9,9-diethyl-7-pyridinylfluoren-2-yl)diphenylamine); N-N = 4,4′-dimethyl-2,2′-bipyridine (**1**), 4,7-dimethyl-1,10-phenanthroline (**2**)) are reported. Both complexes are coordinated by cyclometalated ligands consisting of hole-transporting diphenylamino (DPA)- and fluorene-based 2-phenylpyridine moieties. Structural information on these heteroleptic complexes has been obtained by using an X-ray diffraction study of complex **2**. Complexes **1** and **2** are morphologically and thermally stable ionic solids and are good yellow phosphors at room temperature with relatively short lifetimes in both solution and solid phases. These robust iridium complexes can be thermally vacuum-sublimed and used as phosphorescent dyes for the fabrication of high-efficiency organic light-emitting diodes (OLEDs). These devices doped with 5 wt % **1** can produce efficient electrophosphorescence with a maximum brightness of up to 15 610 cd m^{-2} and a peak external quantum efficiency of ca. 7 % photons per electron that corresponds to a luminance efficiency of ca. 20 cd A^{-1} and a power efficiency of ca. 19 lm W^{-1}. These results show that charged iridium(III) materials are useful alternative electrophosphors for use in evaporated devices in order to realize highly efficient doped OLEDs.

1. Introduction

Advances in organic light-emitting diodes (OLEDs) have triggered intensive research effort towards the development of efficient phosphorescent materials owing to their excellent performance and potential applications in OLEDs for full-color flat-panel display technology and light-emitting electrochemical cells (LECs).[1] Both electrogenerated singlet and triplet excitons can be utilized for light emission in these complexes, with nearly 100 % internal quantum efficiency being attainable.[2] The highly efficient phosphorescence emission is attributed to the strong spin-orbit coupling of the electronic states by the heavy-atom effect of the transition metal which can facilitate the singlet–triplet spin crossover. Among phosphorescent heavy-metal compounds reported, cyclometalated iridium(III) complexes have emerged as the most promising materials for high-performance work because they show intense triplet emission at room temperature and significantly shorter phosphor lifetime when compared with other heavy-metal compounds.[3] The device efficiency and emission color of iridium-based OLEDs can be modified easily by tuning the structure of the organic-ligand chromophore.[3]

For the best performance in display-oriented applications, an Ir^{III} guest can be dispersed in a host material to reduce triplet–triplet annihilation and concentration quenching. In this regard, studies have been inevitably limited to neutral molecules as they are usually more sublimable and compatible with the hydrophobic matrices used.[3] However, compared with neutral complexes, charged Ir^{III} complexes were demonstrated to possess many merits that make them eminent candidates for solid-state lighting and display applications.[3h,4] The power consumption of such OLED devices can be low even using inert metal electrodes and the excellent redox stability of charged iridium complexes can remarkably improve the device stability. They also show good charge-transfer properties. In spite of the impressive scope for the OLED industry that charged complexes can offer, the poor sublimability of the charged iridium complex guest and its inferior compatibility with hydrophobic polymer hosts commonly in use still pose serious problems that could hinder the development of their widespread applications. Although various approaches have been employed to incorporate charged iridium chromophores into non-π-conjugated polymer main chains or side chains via chemical bonds,[5] the use of small-molecule charged iridium emitters in doped or nondoped devices has received scant attention and it was not until recently that electroluminescent devices with spin-coated

[*] Dr. W.-Y. Wong, Dr. G.-J. Zhou
Department of Chemistry and
Centre for Advanced Luminescence Materials
Hong Kong Baptist University
Waterloo Road, Kowloon Tong, Hong Kong (P.R. China)
E-mail: rwywong@hkbu.edu.hk
X.-M. Yu, Prof. H.-S. Kwok
Department of Electronic and Electrical Engineering and
Centre for Display Research
The Hong Kong University of Science and Technology
Clearwater Bay, Hong Kong (P.R. China)
Dr. Z. Lin
Department of Chemistry
The Hong Kong University of Science and Technology
Clearwater Bay, Hong Kong (P.R. China)

[**] This work was supported by a CERG Grant from the Hong Kong Research Grants Council (HKBU2022/03P) and a Faculty Research Grant from the Hong Kong Baptist University (FRG/04-05/II-59).

neat emissive layers of charged iridium complex have been fabricated.[4b,d,6] All other related work reported has proliferated exclusively to the state-of-the-art polymer-based devices where the iridium phosphor is solution-processed with a polymer host using a spin-coating method.[7] To our surprise, there have not been any reports to date exploring charged Ir^{III} phosphors for use as vacuum-evaporable dopants in OLEDs. Presumably, these ionic Ir^{III} complexes, akin to the largely examined cationic Ru^{II} tris(bipyridine) complex $[Ru(bpy)_3]^{2+}(X^-)_2$ (where X^- is an anion such as ClO_4^-, PF_6^-, or BF_4^-) and their derivatives in LECs,[8] are quite unsuitable for the fabrication of conventional, small-molecule OLEDs using the vacuum-deposition method. This can be mainly attributed to poor volatility due to their intrinsic ionic nature, which results in severe thermal degradation during vacuum evaporation. But, for LECs in which the mechanism of operation is dominated by the large amount of ionic charge, they usually require longer response times to achieve steady and maximum emission.[8] Therefore, it is highly desirable that the designed phosphor is a charged species that can also form a uniform good-quality film by vacuum sublimation in the OLED fabrication process. As the first step towards this goal, we report here the synthesis and detailed studies of the light-emitting and electrochemical properties of a new class of phosphorescent cationic iridium complexes containing diphenylaminofluorene units **1** and **2**. These charged complexes are stable with respect to sublimation and thus are suitable for vacuum deposition in phosphorescent OLED fabrication.

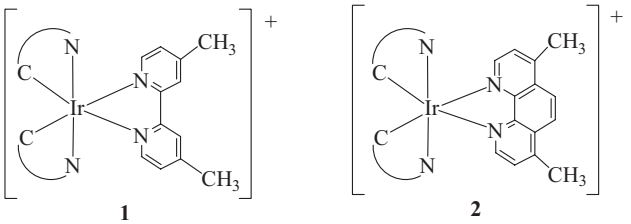

2. Results and Discussion

2.1. Preparation and Chemical Characterization

In the first place, the cyclometalating diphenylaminofluorene-based ligand **HL** can be obtained from the Stille coupling of (7-bromo-9,9-diethylfluoren-2-yl)diphenylamine[9] with 2-(tributylstannyl)pyridine using $[Pd(PPh_3)_4]$ as the catalyst (Scheme 1). It is known that the diphenylamino (DPA) moiety has been widely used for the synthesis of dipolar molecules for various photonic research, including two-photon absorption studies,[9,10] whereas fluorene-based chromophores hold great promises as highly stable and efficient emissive cores in affording novel iridium complexes.[5d,7,11] By introducing a diphenylaminofluorene group as a spacer in the framework of 2-phenylpyridine, Ir^{III} complexes featuring new functional properties can be anticipated. The two-step synthesis of the heteroleptic charged iridium complexes **1** and **2** with different diimine ligands is outlined in Scheme 1, which involves the cyclometalation of $IrCl_3 \cdot nH_2O$ with **HL** to form initially the chloride-bridged dimer $[Ir(\mathbf{L})_2Cl]_2$, followed by reaction with a stoichiometric amount of 4,4′-dimethyl-2,2′-bipyridine or 4,7-dimethyl-1,10-phenanthroline (N-N) and metathesis with NH_4PF_6.[6a,12] In this context, the present method ensures the formation of $[Ir(\mathbf{L})_2(N\text{-}N)]^+$-type species in rather mild conditions compared to other synthetic protocols that usually demand harsher conditions (e.g., reflux in a high-boiling-point solvent) and much longer reaction times. Purification of the mixture by using silica chromatography furnished **1** and **2** as air-stable orange powders in high purity. Both cationic complexes, obtained as PF_6^- salts, are soluble in CH_2Cl_2, $CHCl_3$, and acetone and their solutions remain stable in air for several weeks. The identities of the products were accomplished through NMR spectroscopy and mass spectrometry methods in addition to elemental analysis from which they were shown to consist of well-defined structures. ^1H NMR data suggested that the complexes are always in pure stereoisomeric form (one set of proton signals). Presumably, the proposed coordination at the iridium center is the one containing anionic diphenylaminofluorene-pyridyl ligands with cis-metalated carbon atoms and trans nitrogen atoms, as revealed by previous structural studies on related mononuclear species.[13] This was also verified by a single-crystal X-ray structural analysis of **2** (Fig. 1), the cation of which reveals that the central iridium center is coordinated by two anionic N–C ligands and one neutral chelating N–N ligand. The coordination around Ir(1) is distorted octahedral, with the largest deviation represented by the bite angle of the phenanthroline ligand at 77.4(3)°, which is comparable to the average value of 78.7(8)° reported for $[Ir(bpy)_3]^{3+}$ (bpy = 2,2′-bipyridine). There are no interionic contacts within the lattice. Owing to the higher trans influence of the metalated C(26) atom relative to the pyridyl nitrogen atom N(2A), the Ir(1)–N(3) bond distance (2.147(5) Å) is longer than that for the Ir(1)–N(2) bond (2.053(5) Å). The matrix-assisted laser desorption ionization time-of-flight (MALDI-TOF) mass spectra of **1** and **2** further confirmed the successful formation of the desired complexes which displayed the $(M\text{-}PF_6)^+$ ionic peaks at $m/z = 1308$ and 1332, respectively, and their remarkable stability during the desorption/ionization process.

2.2. Photophysical and Thermal Properties

The thermal stability of **1** and **2** was studied by using thermogravimetric analysis (TGA) measured under a nitrogen stream (Table 1). The complexes have excellent thermal stability and their 5% weight reduction temperatures ($\Delta T_{5\%}$) are comparable to each other: 414 °C for **1** and 418 °C for **2**. In addition, both of them can be thermally evaporated under vacuum without significant decomposition, they both show good film-forming qualities, and are stable toward air oxidation. However, differential scanning calorimetry (DSC) of both

ADVANCED FUNCTIONAL MATERIALS

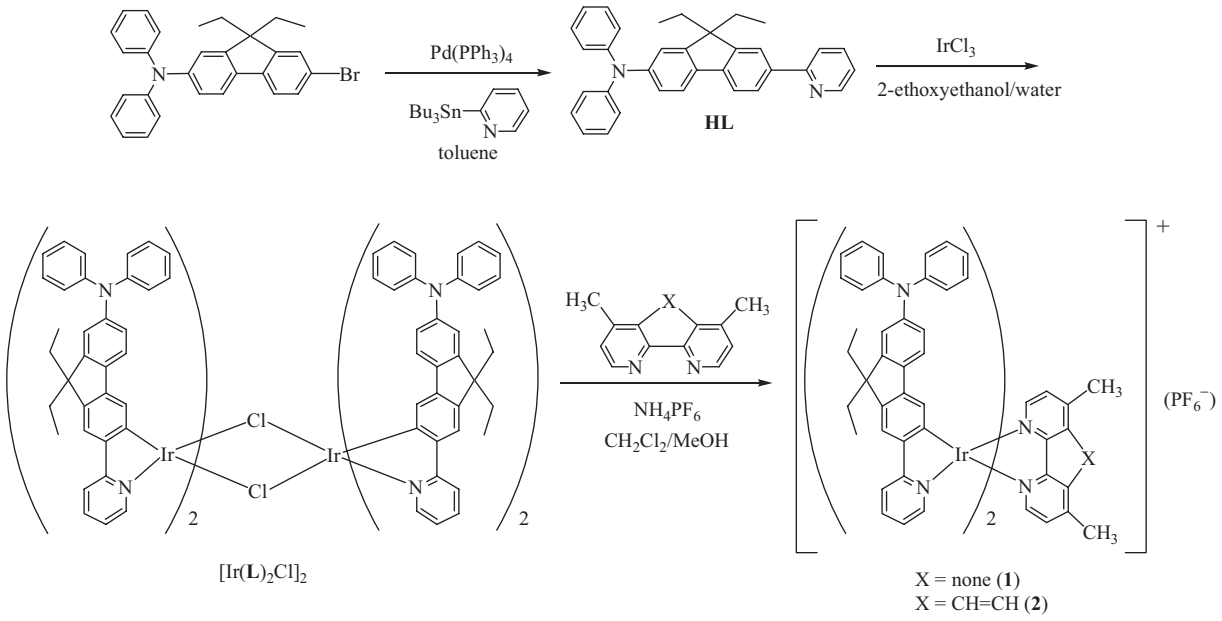

Scheme 1. Synthesis of charged iridium(III) complexes **1** and **2**.

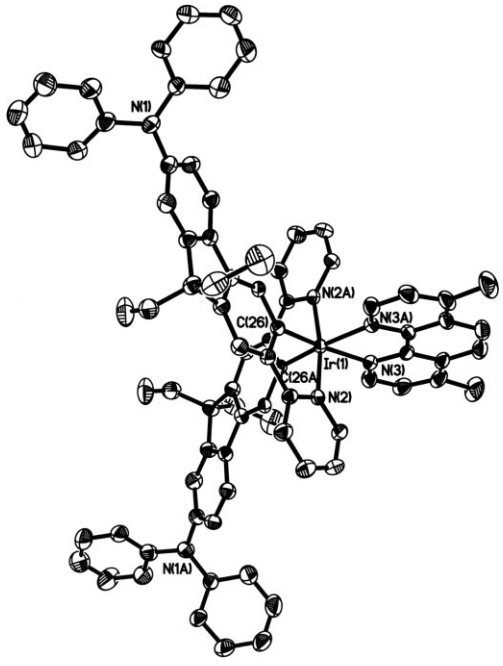

Figure 1. Oak Ridge Thermal Ellipsoid Plot (ORTEP) drawing of the cation of **2** with thermal ellipsoids shown at 25% probability level. Hydrogen atoms are omitted for clarity. Selected distances: Ir(1)–N(2) 2.053(5), Ir(1)–N(3) 2.147(5), Ir(1)–C(26) 1.993(6) Å, and angles: N(2)–Ir(2)–N(3) 98.9(2), N(2)–Ir(1)–N(2A) 170.9(2), N(2)–Ir(1)–C(26) 80.1(2), N(3)–Ir(1)–C(26) 172.6(2), N(3)–Ir(1) –N(3A) 77.4(3)°.

compounds revealed no sign of glass transitions prior to decomposition.

The UV-vis and photoluminescence (PL) spectra of **1** and **2** were recorded (Fig. 2). The absorption spectra of both complexes in dichloromethane solution (Table 1) are characterized by intense bands at $\lambda < 300$ nm ($\log\varepsilon \sim 4.57$-$4.89$) which are attributed mainly to the spin-allowed $^1\pi$–π^* ligand-centered (LC) transitions due to contributions from functionalized phenylpyridyl and diimine moieties. Moderately intense bands at longer wavelengths also extend far within the visible region from 402 to 443 nm, corresponding to electronic excitation to the spin-allowed singlet metal-to-ligand charge-transfer (^{1}MLCT), and spin-forbidden triplet metal-to-ligand charge-transfer (^{3}MLCT) and LC $^3\pi$–π^* states. Observation of the ^{3}MLCT and $^3\pi$–π^* bands is caused by the large spin-orbital coupling induced by the heavy-metal iridium center. Emission in these mixed-ligand systems can actually be attributed to strong mixing between the MLCT and LC excited states. A similar discussion has been previously used for analogous cyclometalated iridium complexes reported in the literature.[3] These assignments were also supported by using density functional theory (DFT) calculations for **2**, and the contour plots depicted in Figure 3 show that the highest occupied molecular orbitals (HOMO and HOMO-1) are derived from the π orbitals of the arylamine structural moieties of the two N–C bidenate ligands. The HOMO-2 level contains substantial contribution from the iridium center and corresponds to a linear combination of a metal d orbital (28.9% Ir(d)) and the π orbitals from the two iridium-bonded phenyl rings. The lowest unoccupied molecular orbitals (LUMO and LUMO+1) are the π* orbitals of the phenanthroline ligand. It is obvious that the HOMO and LUMO orbitals are orthogonal to each other, and thus, there is little electronic overlap between them. While the ligand **HL** fluoresces at 446 nm, both iridium diimine complexes **1** and **2** emit strong phosphorescence (λ_{em} in $CH_2Cl_2 = 568$ and 570 nm for **1** and **2**, respectively) from the triplet excited state at room temperature in fluid solution and at 77 K in a rigid matrix, accompanied by large Stokes shifts (>100 nm). No fluorescence could be detected for either complex. Both the absorption and phosphorescence spectra of **1** appear at wavelengths

Table 1. Photophysical and thermal data for **1** and **2**.

	Absorption @ 293 K	Emission @ 293 K							$\Delta T_{5\%}$ [°C]
	λ_{abs} CH_2Cl_2 [nm] [a]	λ_{em} CH_2Cl_2 [nm]	λ_{em} film [nm]	Φ_P [b]	τ_P [μs] [c]	k_r [s^{-1}]	k_{nr} [s^{-1}]	τ_P [μs] [d]	
1	264 (4.69)	568	576	0.11	0.02	5.5×10^6	4.5×10^7	1.57	414
	297 (4.69)	603sh	605sh		(0.18)			(30.2)	
	402 (4.65)								
	443 (4.57)								
2	270 (4.89)	570	579	0.05	0.01	5.0×10^6	9.5×10^7	1.40	418
	298 (4.85)	605sh	610sh		(0.20)			(36.8)	
	403 (4.83)								
	441 (4.71)								

[a] Logε values are shown in parentheses. [b] Measured in degassed CH_2Cl_2 relative to *fac*-[Ir(ppy)$_3$] ($\Phi_P = 0.40$). [c] Measured in CH_2Cl_2 at 293 K in air. The radiative lifetimes τ_r (μs) are shown in parentheses. [d] Solid state at 293 K. Numbers in parentheses were obtained at 77 K in a frozen CH_2Cl_2 matrix. sh = shoulder.

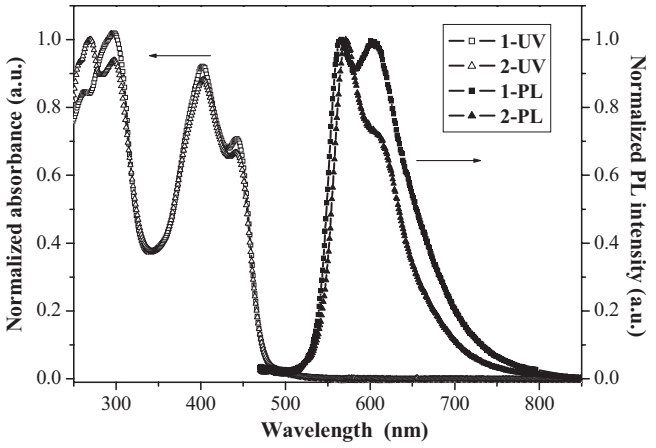

Figure 2. Normalized absorption and PL spectra of **1** and **2** in CH_2Cl_2 at 293 K.

(λ_{abs} = 264, 297, 402, 443 nm, λ_{em}(film) = 576 nm) longer than those of $[Ir(ppy)_2(C_9\text{-bpy})]^+$ (ppy = 2-phenylpyridine, C_9-bpy = 4,4′-di-*n*-nonyl-2,2′-bipyridine) without the DPA units (= 257, 305sh, 338sh nm, λ_{em}(film) = 552 nm).[12] Integration of a DPA electron-donor group with the electron-deficient pyridine moiety increases the intramolecular donor–acceptor character of the ligand in **1** and **2**, leading to a red-shift of their phosphorescence peak maxima. Apparently, the color of light emission from **1** and **2** is not very sensitive to the type of diimine ligands used in the present study and complex **1** has a very similar emission pattern to its analogue **2**. The phosphorescence quantum yields, Φ_P, in CH_2Cl_2 solutions excited at 403 nm are moderate at 0.11 and 0.05 for **1** and **2**, respectively, relative to a *fac*-[Ir(ppy)$_3$] standard ($\Phi_P = 0.40$)[14] which are found to be higher than that found for $[Ir(ppy)_2(C_9\text{-bpy})]^+$ (~0.03).[12] Luminescence decays are monoexponential and are in the microsecond time scale. The phosphorescence lifetimes, τ_P, have a magnitude of about 0.01–0.02 μs in CH_2Cl_2, shorter than those of $[Ir(ppy)_2(C_9\text{-bpy})]^+$ (0.07 μs)[12] and most of the other reported complexes of this kind. Accordingly, the radiative lifetimes (τ_r) of the triplet excited state deduced from $\tau_r = \tau_P/\Phi_P$ are as short as 0.18–0.20 μs,[3k] which correlates well with the unusually large extinction coefficients measured for triplet-state absorption bands. In the solid state, the lifetime is also short (1.40–1.57 μs), possibly due to the phosphorescence self-quenching associated with molecular packing. The τ_P values at 77 K are longer than those at 293 K. As the intersystem crossing (ISC) efficiency (Φ_{ISC}) can be roughly taken to be 100 % for heavy iridium chromophores,[15] the triplet radiative and non-radiative rate constants, k_r and k_{nr}, are calculated from Φ_P and τ_P using the equations $k_{nr} = (1 - \Phi_P)/\tau_P$ and $k_r = \Phi_P/\tau_P$. Clearly, complexes **1** and **2** have the same order of magnitudes for the k_r and k_{nr} values.

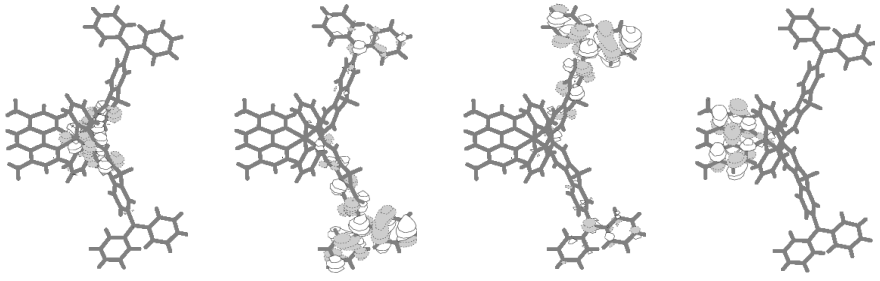

Figure 3. Contour plots of the highest occupied (HOMO-2, HOMO-1, and HOMO) and lowest unoccupied (LUMO) molecular orbitals for **2**.

2.3. Electrochemical and Electronic Characterization

The redox properties of **1** and **2** were investigated by using cyclic voltammetry (Table 2). The ligand **HL** displayed the anodic and cathodic waves at 0.54 and –1.79 V, respectively. The ligand redox behavior are affected by cyclometalation and complexes **1** and **2** are both easier to oxidize and harder to reduce when compared to **HL**. Both of them show two reversible anodic redox couples that are assigned to the oxidation of the peripheral

Table 2. Electrochemical properties and frontier orbital energy levels of **1** and **2**.

Complex	$E_{1/2}^{ox}$ [V] [a]	$E_{1/2}^{red}$ [V] [a]	HOMO [eV]	LUMO [eV]	E_g [eV] [b]	E_g [eV] [c]
1	0.42, 1.01	–1.91	–5.22	–2.89	2.33	2.63
2	0.40, 1.00	–1.88	–5.20	–2.92	2.28	2.63

[a] 0.1 M $[Bu_4N]PF_6$ in tetrahydrofuran, scan rate 100 mV s^{-1}, versus Fc/Fc^+ couple. [b] E_g = LUMO – HOMO. [c] Estimated from the onset wavelength of the solid-state optical absorption.

arylamino group followed by the removal of an electron from the Ir–C^- σ-bonding orbitals of the bis-cyclometalated phenyl-Ir center. Cathodic sweeps show an irreversible wave at –1.91 and –1.88 V for **1** and **2**, respectively, presumably due to reduction of the diimine group,[12,13a] which is consistent with the DFT results for **2**. The reduction of the **L** group is not apparent within the solvent window. From the redox data, we can estimate the HOMO and LUMO energy levels of **1** and **2** with reference to the energy level of ferrocene (4.8 eV below the vacuum level) and the first oxidation potentials were used to determine the HOMO energy levels.[16] The HOMO and LUMO levels for **1** and **2** match very closely with the energy levels for 4,4′-bis[*N*-(1-naphthyl)-*N*-phenylamino]biphenyl (NPB, HOMO: –5.2 eV) and 2,2′,2″-(1,3,5-phenylene)tris(1-phenyl-1*H*-benzimidazole) (TPBI, LUMO: –2.9 eV). The LUMO levels of **1** and **2** (–2.89 and –2.92 eV), which are lower than that of 2-(4-biphenylyl)-5-(4-*tert*-butylphenyl)-1,3,4-oxadiazole (PBD, –2.4 eV),[17] one of the most widely used hole-blocking/electron-transport material and comparable to that of tris(8-hydroxyquinolinato)aluminum (Alq_3, –3.0 eV), indicate their good electron-transporting features. Accordingly, as elaborated below, the performance of the OLED devices prepared from these complexes was expected to be promising.

2.4. Electrophosphorescent Device Properties

Organometallic phosphors **1** and **2** have very good film- and glass-forming properties for accessing their electrophosphorescent ability in evaporated devices. Presumably, because they have two bulky and robust diphenylaminofluorene cores that completely surround the Ir^{3+} ions, weaker interactions between adjacent iridium molecules tend to increase the volatility of these ionic complexes, enabling them to sublime easily (ca. 210–215 °C at a pressure of 2×10^{-4} Pa) before decomposition during the vacuum thermal evaporation. These phosphors are better used as a phosphorescent dopant rather than a single emission layer in OLEDs to prevent the severe self-quenching expected in the solid. Because of the higher PL quantum efficiency of **1**, OLED devices **A**–**C** were fabricated using **1** as the dopant at three different doping concentrations. Complex **1** is sufficiently stable with respect to sublimation for a fabrication process using the vacuum-deposition method and the identical PL spectrum of the vacuum-sublimed dopant in CBP with the spin-coated neat film PL confirms that the same chemical species are involved in both cases. Figure 4 depicts the general four-layer structures for the electrophosphorescent devices and the molecular structures of the compounds employed. 4,4′-*N*,*N*′-Dicarbazolebiphenyl (CBP) acts as a small-molecule host

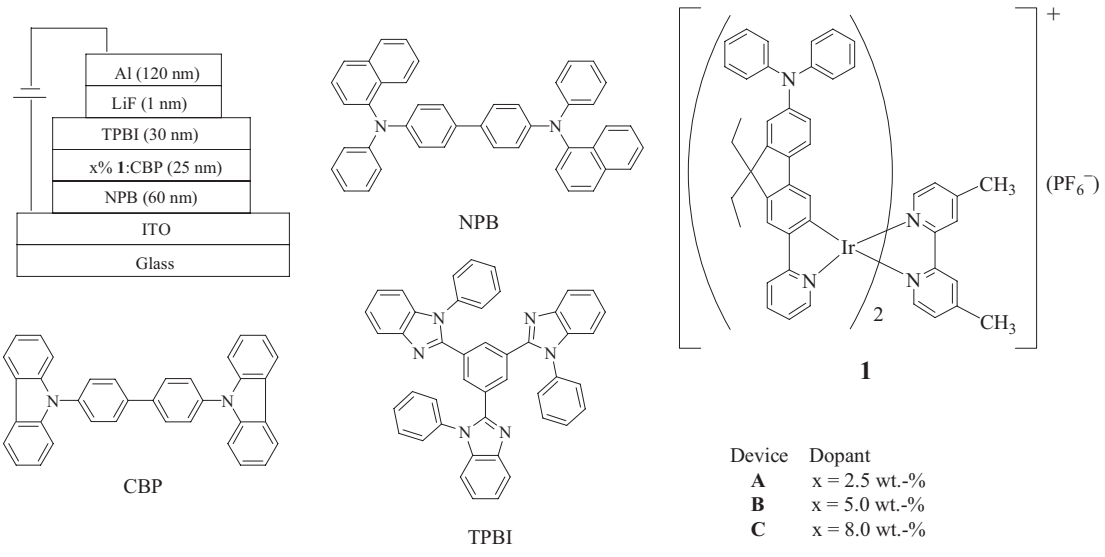

Figure 4. The general structure for OLED devices and the molecular structures of the relevant compounds used in these devices. TPBI, CBP: 4,4′-*N*,*N*′-dicarbazolebiphenyl, NPB, and ITO: indium tin oxide.

material for the electrophosphor, NPB as a hole-transport layer, TBPI as both a hole blocker and an electron transporter, and LiF as an electron-injection layer. Here, TBPI, instead of the commonly used 2,9-dimethyl-4,7-diphenyl-1,10-phenanthroline (BCP) or Alq_3, was adopted for the devices to confine excitons within the emissive zone since it shows a higher electron mobility.[18] We chose CBP as the host layer for device fabrication because of the excellent overlap of the UV-vis absorption of these iridium complexes with the PL spectrum of CBP, and such guest–host systems allow efficient Förster energy transfer from the CBP host singlet to the iridium guest complex. To optimize the device efficiency, a concentration-dependence experiment was carried out in the range between 2.5 and 8.0 wt %. It is worth noting that even at high current densities, emission from CBP is negligible in all cases, indicating complete energy and/or charge transfer from the host exciton to the phosphor molecule upon electrical excitation. Pertinent performance characteristics of the devices **A**–**C** are summarized in Table 3. Figure 5 shows the electroluminescence (EL) spectra of devices **B** and **C** at a driving voltage of 8 V. The EL spectra for the devices exhibited no significant change with variation of the operating bias voltage from 6 to 12 V, and the maximum EL peak is independent of the dopant concentration. Essentially, each of the devices **A**–**C** exhibits a prominent EL emission peak at about 565 nm with low turn-on voltages ($V_{\text{turn-on}}$) for light emission at 1 cd m^{-2} of 5.0–5.5 V. However, there is a minor NPB emission band at the low doping level (2.5 wt %) in device **A**. The Commission Internationale de L'Eclairage (CIE) color coordinates are (0.44, 0.47) for device **B** and (0.44, 0.48) for device **C** and both values correspond to the yellow region of the CIE chromaticity diagram. In each case, the EL spectrum resembles its corresponding PL spectrum from a thin film, indicating that the same optical transition is responsible for light emission and no chemical change of the compounds occurs during the EL process. Clearly, there is also no sign of metal-complex aggregation in these devices.

Figure 6a and b shows the current density and luminance versus bias voltage curves of the charged iridium-doped OLEDs at three different doping concentrations of **1**. In general, the brightness of the devices at a given current density shows a slight increase as the dopant concentration is increased

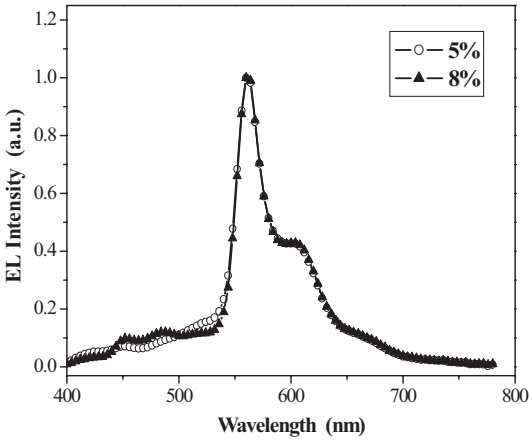

Figure 5. EL spectra of **1**-doped OLEDs at 5 and 8 wt % dopant level at 8 V.

from 2.5 to 8.0 wt %. The light output reached 15 534–18 763 cd m^{-2} at 12.1 V for devices **A**–**C**. The external quantum efficiency, luminance efficiency, and power efficiency of the 5 % doped device as a function of current density are presented in Figure 7a and b. A maximum external quantum efficiency ($\eta_{\text{ext.}}$) of 6.48 %, a luminance efficiency (η_{L}) of 19.72 cd A^{-1}, and a power efficiency (η_{p}) of 18.39 lm W^{-1} at 3.4 V are realized in device **B**. For devices **A** and **C**, the corresponding peak efficiencies are $\eta_{\text{ext.}} = 3.19\,\%$, $\eta_{\text{L}} = 5.91$ cd A^{-1}, and $\eta_{\text{p}} = 3.87$ lm W^{-1}, and $\eta_{\text{ext.}} = 5.21\,\%$, $\eta_{\text{L}} = 16.13$ cd A^{-1}, and $\eta_{\text{p}} = 15.78$ lm W^{-1}, respectively. At the low concentrations, the $\eta_{\text{ext.}}$ value increases with increasing concentrations of the dopant. At high concentrations beyond 5 wt %, $\eta_{\text{ext.}}$ tends to decrease slightly, probably as a consequence of concentration quenching and the maximum $\eta_{\text{ext.}}$ was achieved at 5 wt % concentration. In common with most phosphorescent devices, there was a decrease in efficiency with increasing current density, which has been attributed to a combination of triplet–triplet annihilation[19] and field-induced quenching effects.[20] For **1**, at 5 wt % doping level (device **B**) and a practical current density of 20 mA cm^{-2}, the external quantum efficiency is 2.47 % with a luminance efficiency of 7.42 cd A^{-1}, whereas at a higher current density of 100 mA cm^{-2}, the quantum and lumi-

Table 3. Performance of electrophosphorescent OLEDs based on charged Ir^{III} complex **1**.

Device	Phosphor dopant (wt %)	$V_{\text{turn-on}}$ [V]	Luminance L [cd m^{-2}]	η_{ext} [%]	η_{L} [cd A^{-1}]	η_{p} [lm W^{-1}]	λ_{max} [nm]
A	**1** (2.5)	5.5	888 [a]	1.73	3.24	1.45	450 [d], 565
			3005 [b]	1.30	2.43	0.91	
			15534 (12.1) [c]	3.19 (5.3)	5.91 (5.3)	3.87 (4.5)	
B	**1** (5.0)	5.0	1498 [a]	2.47	7.42	3.36	565
			4779 [b]	1.57	4.78	1.68	
			15611 (12.1) [c]	6.48 (3.4)	19.72 (3.4)	18.39 (3.3)	
C	**1** (8.0)	5.1	1597 [a]	2.60	7.96	3.70	565
			5197 [b]	1.69	5.23	1.95	
			18763 (12.1) [c]	5.21 (3.4)	16.13 (3.4)	15.78 (3.1)	

[a] Values collected at 20 mA cm^{-2}. [b] Values collected at 100 mA cm^{-2}. [c] Maximum values of the devices. Values in parentheses are the voltages at which they were obtained. [d] A minor NPB emission peak.

ADVANCED FUNCTIONAL MATERIALS

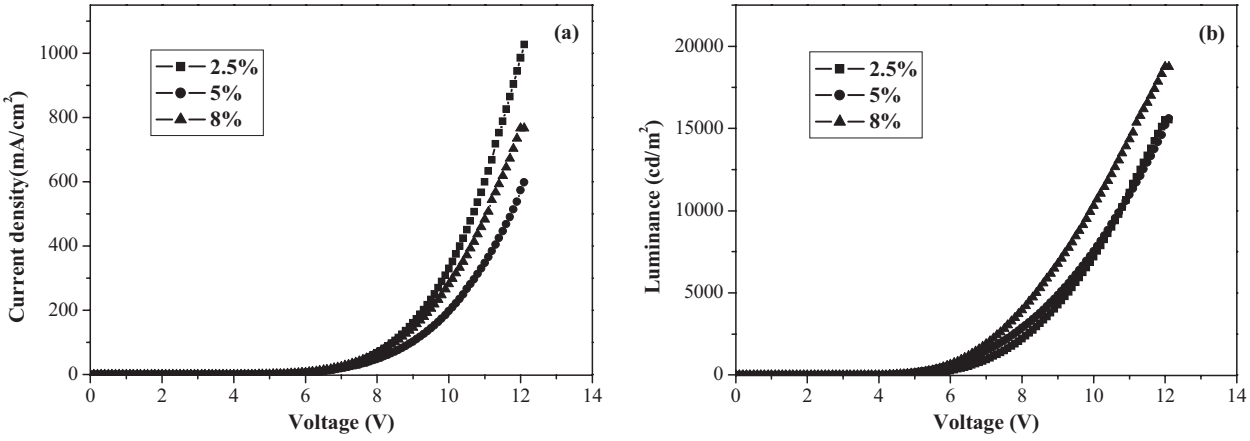

Figure 6. a) Current density–voltage and b) luminance–voltage characteristics of three electrophosphorescent OLED devices **A**–**C** with various doping concentrations of **1** in CBP.

nance efficiencies gradually drop to 1.57 % and 4.78 cd A^{-1}, respectively. This corresponds to a loss of 36 % in emission efficiency. The corresponding losses of 25 and 35 % in η_{ext} were noted for devices **A** and **C**.

3. Conclusions

We have accomplished the synthesis and investigated the light-emitting properties of some charged iridium complexes of a diphenylaminofluorene-type fluorophore which exhibit good thermal and morphological stability. The results were satisfactorily correlated with the X-ray structural and theoretical DFT data. Variation of the diimine ligands does not seem to change the PL and redox properties much. For the first time in the electrophosphorescent OLED area, these charged metal phosphors with relatively short lifetimes in both solution and solid phases can be vacuum-evaporated without decomposition. Presumably due to the intrinsically ionic nature of our new complexes, devices fabricated from **1** as a dopant emitted strong yellow light ($\lambda_{max} = 565$ nm) with a brightness exceeding 15 000 cd m^{-2} and luminance and power efficiencies as high as 20 cd A^{-1} and 19 lm W^{-1}, respectively at the 5 % doping level. The current strategy is very promising for the continual development of using vacuum-sublimable charged iridium phosphors for high-efficiency OLEDs.

4. Experimental

General Information: All reactions were performed under nitrogen. Solvents were carefully dried and distilled from appropriate drying agents prior to use. Commercially available reagents were used without further purification unless otherwise stated. The procedure for the synthesis of (7-bromo-9,9-diethylfluoren-2-yl)diphenylamine and **HL** followed the methods reported in the literature [3p,9]. All reactions were monitored by using thin-layer chromatography (TLC) with Merck precoated glass plates. Compounds were visualized with UV-light irradiation at 254 and 365 nm. Flash column chromatography and preparative TLC were carried out using silica gel from Merck (230–400 mesh). MALDI-TOF mass spectra were obtained on a Autoflex Bruker MALDI-TOF system. NMR spectra were measured in appropriate deuterated solvents on a Varian Inova 400 MHz Fourier transform NMR spectrometer; chemical shifts were quoted relative to the internal standard tetramethylsilane for ^{1}H and $^{13}C\{^{1}H\}$ NMR data.

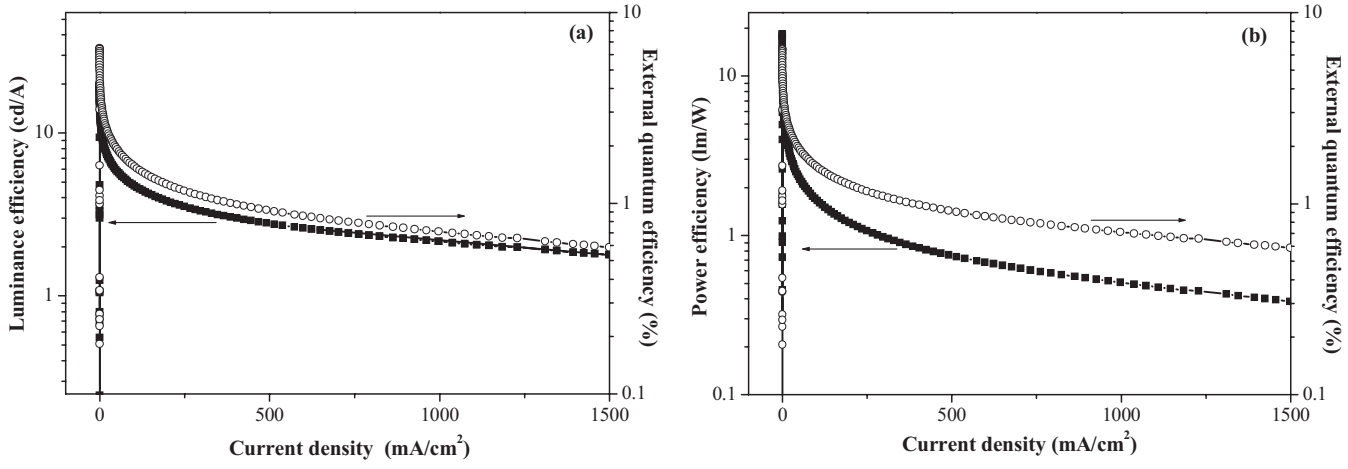

Figure 7. External quantum, luminance, and power efficiencies as a function of current density for OLED device **B** using 5 wt % of guest dopant **1**.

Physical Measurements: UV-vis spectra were obtained on a HP-8453 spectrophotometer. The photoluminescent properties and lifetimes of the compounds were probed on the Photon Technology International (PTI) Fluorescence Master Series QM1 system. The phosphorescence quantum yields were determined in CH_2Cl_2 solutions at 293 K against *fac*-[Ir(ppy)$_3$] as a reference ($\Phi_P = 0.40$) [14]. For solid-state emission spectral measurements, the 325 nm line of a He–Cd laser was used as an excitation source. The luminescence spectra were analyzed using a 0.25 m focal length double monochromator with a Peltier cooled photomultiplier tube and processed with a lock-in-amplifier. Electrochemical measurements were recorded using a BAS CV-50W model potentiostat. A conventional three-electrode configuration consisting of a Pt working electrode, a Pt wire counter electrode, and an Ag/AgCl reference electrode was used. The solvent in all measurements was tetrahydrofuran THF, and the supporting electrolyte was 0.1 M $[Bu_4N]PF_6$. Ferrocene was added as a calibrant after each set of measurements, and all potentials reported were quoted with reference to the ferrocene–ferrocenium (Fc/Fc^+) couple at a scan rate of 100 mV s^{-1}. Thermal analyses were performed with the Perkin–Elmer Pyris Diamond DSC and Perkin–Elmer TGA6 thermal analyzers. Density functional calculations at the B3LYP level were performed with the use of Gaussian 03 [21] on the basis of the experimental geometry obtained from the X-ray data. The four ethyl groups were replaced with hydrogen atoms. The basis set used for C, N, O, and H atoms was 6-31G, whereas effective core potentials with a LanL2DZ basis set were employed for the iridium atom [22]. All the molecular-orbital plots were made with the use of Molden 3.5 [23].

*Preparation of **HL***: (7-Bromo-9,9-diethylfluoren-2-yl)diphenylamine (2.30 g, 4.91 mmol) and 2-(tributylstannyl)pyridine (2.07 g, 5.62 mmol) were mixed in dry toluene (50 mL) and $Pd(PPh_3)_4$ (0.58 g, 0.50 mmol) was added to the solution. The reaction mixture was stirred at 110 °C for 24 h. After cooling to room temperature, the reaction mixture was poured into a separating funnel and CH_2Cl_2 (200 mL) was added followed by washing with water (3 × 100 mL). The organic phase was then dried over $MgSO_4$. After the removal of solvent, the residue was purified by using column chromatography eluting with CH_2Cl_2/hexane (3:1, v/v) to give the title product as a yellow solid in 79 % yield (1.80 g).

Spectral Data: MS (FAB): *m*/*z* 466 (M^+). ^{1}H NMR (400 MHz, $CDCl_3$, 293 K): δ [ppm]: 8.70 (d, J = 4.6 Hz, 1H, Ar), 7.98–7.58 (m, 6H, Ar), 7.27–6.97 (m, 13H, Ar), 2.07–1.91 (m, 4H, Et), 0.38 (t, J = 7.3 Hz, 6H, Et). ^{13}C{^{1}H} NMR (100.6 MHz, $CDCl_3$, 293 K): δ [ppm]: 157.64, 151.71, 150.31, 149.44, 147.81, 147.30, 142.18, 137.31, 136.49, 135.98, 129.05, 125.81, 123.76, 123.44, 122.42, 121.60, 121.01, 120.54, 120.38, 119.15, 119.13, 56.27, 32.72, 8.71. Anal. calcd. for $C_{34}H_{30}N_2$: C, 87.52; H, 6.48; N, 6.00; found: C, 87.25; H, 6.26; N, 5.78.

*Preparation of [Ir(**L**)$_2$(N-N)] (N-N = 4,4′-dimethyl-2,2′-bipyridine) (**1**)*: The cyclometalating ligand **HL** (500.0 mg, 1.07 mmol) and $IrCl_3 \cdot nH_2O$ (100.0 mg, 54 wt % iridium content) were added to a mixture of 2-ethoxyethanol and water (10 mL, 3:1, v/v). The reaction mixture was stirred at 120 °C for 18 h and after cooling to room temperature, a yellow precipitate was obtained. The precipitate was collected and washed with ethanol (20 mL) and hexane (10 mL). Subsequently, the cyclometalated iridium dimer $[Ir(\mathbf{L})_2Cl]_2$ was dried under vacuum and isolated as a yellow solid (280.0 mg, 85 %). $[Ir(\mathbf{L})_2Cl]_2$ (175.0 mg, 0.076 mmol) and 4,4′-dimethyl-2,2′-bipyridine (27.7 mg, 0.150 mmol) were then combined in a CH_2Cl_2–MeOH mixture (10 mL, 2:1, v/v) and the reaction mixture was heated to reflux for 3 h. After cooling to room temperature, a solution of NH_4PF_6 in MeOH (130.0 mg in 1 mL) was added and the resulting mixture was allowed to stir for another 4 h. The solvent was then removed under vacuum and the residue was dissolved in CH_2Cl_2 followed by filtration to remove the insoluble ionic salt. Upon removal of the solvent, the crude product was purified by using column chromatography, first eluting with pure CH_2Cl_2 to get rid of the impurity and then ethyl acetate to isolate the target product. Complex **1** was obtained as an orange solid in 15 % yield (33.0 mg).

Spectral Data: MS (FAB): *m*/*z* 1308 ($[M\text{-}PF_6]^+$). ^{1}H NMR (400 MHz, d_6-acetone, 293 K): δ [ppm] 8.72 (s, 2H, Ar), 8.34 (d, J = 8.4 Hz, 2H, Ar), 8.01–7.94 (m, 6H, Ar), 7.88 (d, J = 5.9 Hz, 2H, Ar), 7.49 (d, J = 5.7 Hz, 2H, Ar), 7.30–7.14 (m, 12H, Ar), 7.08–6.99 (m, 14H, Ar), 6.91–6.87 (m, 2H, Ar), 6.72 (s, 2H, Ar), 2.59 (s, 6H, Me), 2.04 (m, 8H, CH_2CH_3), 0.41 (t, J = 7.3 Hz, 6H, CH_2CH_3), 0.21 (t, J = 7.3 Hz, 6H, CH_2CH_3). Anal. calcd. for $C_{80}H_{70}N_6F_6PIr$: C, 66.15; H, 4.86; N, 5.79; found: C, 66.10; H, 4.58; N, 5.44.

*Preparation of [Ir(**L**)$_2$(N-N)] (N-N = 4,7-dimethyl-1,10-phenanthroline) (**2**)*: Compound **2** was prepared in a similar manner as described for **1** except that 4,7-dimethyl-1,10-phenanthroline was used instead of 4,4′-dimethyl-2,2′-bipyridine. Following the same work up procedures as above, the crude product was purified by using column chromatography, first eluting with pure CH_2Cl_2 followed by a mixture of CH_2Cl_2–ethyl acetate to afford **2** as an orange powder in 24 % yield.

Spectral Data: MS (FAB): *m*/*z* 1332 ($[M\text{-}PF_6]^+$). ^{1}H NMR (400 MHz, $CDCl_3$, 293 K): δ [ppm] 8.36 (s, 2H, Ar), 8.12 (d, J = 5.1 Hz, 2H, Ar), 7.92 (d, J = 8.1 Hz, 2H, Ar), 7.70 (t, J = 7.6 Hz, 2H, Ar), 7.60 (s, 2H, Ar), 7.52 (d, J = 5.4 Hz, 2H, Ar), 7.38 (d, J = 5.4 Hz, 2H, Ar), 7.23–6.84 (m, 28H, Ar), 6.65 (s, 2H, Ar), 2.96 (s, 6H, Me), 2.02–1.86 (m, 8H, CH_2CH_3), 0.47 (t, J = 7.2 Hz, 6H, CH_2CH_3), 0.29 (t, J = 7.2 Hz, 6H, CH_2CH_3). ^{13}C{^{1}H} NMR (100.6 MHz, $CDCl_3$, 293 K): δ [ppm] 168.18, 152.37, 150.09, 149.75, 148.83, 148.67, 147.83, 146.68, 146.57, 144.23, 143.79, 141.66, 137.48, 135.87, 131.11, 129.14, 127.04, 124.04, 124.83, 123.81, 123.35, 122.57, 122.34, 121.97, 120.62, 119.28, 119.16, 119.14, 55.56, 32.80, 32.65, 19.20, 8.87, 8.72. Anal. calcd. for $C_{82}H_{70}N_6F_6PIr$: C, 66.70; H, 4.78; N, 5.69; found: C, 66.49; H, 4.58; N, 5.40.

*Crystal Data for **2***: $C_{82}H_{70}N_6F_6PIr \cdot 2CHCl_3$, M_w = 1715.35, monoclinic, space group *Cmca*, a = 27.181(1), b = 20.2108(8), c = 32.497(1) Å, V = 17 852(1) Å^3, Z = 8, ρ_{calcd} = 1.276 mg m^{-3}, μ(Mo Kα) = 1.748 mm^{-1}, $F(000)$ = 6928, T = 293 K. 43 483 reflections measured, of which 7963 were unique (R_{int} = 0.0528). Final R_1 = 0.0431 and wR_2 = 0.1161 for 4544 observed reflections with $I > 2\sigma(I)$. The crystallographic data for complex **2** (excluding structure factors) has been deposited in the Cambridge Crystallographic Data Centre with the deposition number CCDC 604219. These data can be obtained free of charge on application to CCDC, 12 Union Road, Cambridge CB2 1EZ, UK (fax: (+44)1223-336-033; E-mail: deposit@ccdc.cam.ac.uk).

OLED Fabrication and Measurements: Commercial indium tin oxide (ITO) coated glass with sheet resistance of 20–30 Ω/square was used as the starting substrate. Before device fabrication, the ITO glass substrates were cleaned by ultrasonic baths in organic solvents followed by ozone treatment for 10 min. Each device was assembled in the following sequence: ITO on a glass substrate (anode), 60 nm of NPB, 25 nm of the emitting layer made of the CBP host and phosphorescent dopant (x %), 30 nm of TPBI, 1 nm of LiF, and 120 nm of Al (cathode). The organic layers were evaporated and laminated in the above sequence under 4×10^{-4} Pa without breaking vacuum between each vacuum-deposition process. The emissive layer was formed by codeposition of the dopant and the host. The evaporation rates were 1–2, 0.3, and 4–6 Å s^{-1} for organic materials, LiF, and aluminum, respectively. The layer thickness was monitored in situ using a quartz crystal oscillator. The active area of the device was 5 mm^2 as defined by the shadow mask. The electrical and optical characteristics of these devices were measured using an R6145 DC voltage current source, FLUKE 45 dual display multimeter and Spectrascan PR650 spectrophotometer in a dark room under ambient air conditions.

Received: April 20, 2006
Revised: June 16, 2006
Published online: January 5, 2007

[1] a) M. A. Baldo, D. F. O'Brien, Y. You, A. Shoustikov, S. Sibley, M. E. Thompson, S. R. Forrest, *Nature* **1998**, *395*, 151. b) M. A. Baldo, M. E. Thompson, S. R. Forrest, *Pure Appl. Chem.* **1999**, *71*, 2095. c) M. A. Baldo, M. E. Thompson, S. R. Forrest, *Nature* **2000**, *403*, 750. d) X. Gong, M. R. Robinson, J. C. Ostrowki, D. Moses, G. C. Bazan, A. J. Heeger *Adv. Mater.* **2002**, *14*, 581. e) S. Welter, K. Brunner, J. W. Hofstraat, L. De Cola, *Nature* **2003**, *42*, 54. f) A. Köhler, J. S. Wilson, R. H. Friend, *Adv. Mater.* **2002**, *14*, 701. g) J. G. C. Veinot, T. J. Marks, *Acc. Chem. Res.* **2005**, *38*, 632.

[2] a) C. Adachi, M. A. Baldo, M. E. Thompson, S. R. Forrest, *J. Appl. Phys.* **2001**, *90*, 5048. b) F. C. Chen, Y. Yang, *Appl. Phys. Lett.* **2002**, *80*, 2308. c) E. Holder, B. M. W. Langeveld, U. S. Schubert, *Adv. Mater.* **2005**, *17*, 1109.

[3] a) S.-J. Yeh, M.-F. Wu, C.-T. Chen, Y.-H. Song, Y. Chi, M.-H. Ho, S.-F. Hsu, C. H. Chen, *Adv. Mater.* **2005**, *17*, 285. b) C.-L. Li, Y.-J. Su, Y.-T. Tao, P.-T. Chou, C.-H. Chien, C.-C. Cheng, R.-S. Liu, *Adv. Funct. Mater.* **2005**, *15*, 387. c) D. K. Rayabarapu, B. M. J. S. Paulose, J.-P. Duan, C.-H. Cheng, *Adv. Mater.* **2005**, *17*, 349. d) Y.-H. Song, S.-J. Yeh, C.-T. Chen, Y. Chi, C.-S. Liu, J.-K. Yu, Y.-H. Hu, P.-T. Chou, S.-M. Peng, G.-H. Lee, *Adv. Funct. Mater.* **2004**, *14*, 1221. e) H. Z. Xie, M. W. Liu, O. Y. Wang, X. H. Zhang, C. S. Lee, L. S. Hung, S. T. Lee, P. F. Teng, H. L. Kwong, H. Zheng, C. M. Che, *Adv. Mater.* **2001**, *13*, 1245. f) J. M. Lupton, I. D. W. Samuel, M. J. Frampton, R. Beavington, P. L. Burn, *Adv. Funct. Mater.* **2001**, *11*, 287. g) C.-L. Lee, R. R. Das, J.-J. Kim, *Chem. Mater.* **2004**, *16*, 4642. h) M. K. Nazeeruddin, R. Humphry-Baker, D. Berner, S. Rivier, L. Zuppiroli, M. Graetzel, *J. Am. Chem. Soc.* **2003**, *125*, 8790. i) H.-C. Li, P.-T. Chou, Y.-H. Hu, Y.-M. Cheng, R.-S. Liu, *Organometallics* **2005**, *24*, 1329. j) K. R. Justin Thomas, M. Velusamy, J. T. Lin, C.-H. Chien, Y.-T. Tao, Y. S. Wen, Y.-H. Hu, P.-T. Chou, *Inorg. Chem.* **2005**, *44*, 5677. k) W.-S. Huang, J.-T. Lin, C.-H. Chien, Y.-T. Tao, S.-S. Sun, Y.-S. Wen, *Chem. Mater.* **2004**, *16*, 2480. l) S. Okada, K. Okinaka, H. Iwawaki, M. Furugori, M. Hashimoto, T. Mukaide, J. Kamatani, S. Igawa, A. Tsuboyama, T. Takiguchi, K. Ueno, *Dalton Trans.* **2005**, 1583. m) P. Coppo, E. A. Plummer, L. De Cola, *Chem. Commun.* **2004**, 1774. n) I. R. Laskar, T.-M. Chen, *Chem. Mater.* **2004**, *16*, 111. o) T.-H. Kwon, H. S. Cho, M. K. Kim, J.-W. Kim, J.-J. Kim, K. H. Lee, S. J. Park, I.-S. Shin, H. Kim, D. M. Shin, Y. K. Chung, J.-I. Hong, *Organometallics* **2005**, *24*, 1578. p) W.-Y. Wong, G.-J. Zhou, X.-M. Yu, H.-S. Kwok, B.-Z. Tang, *Adv. Funct. Mater.* **2006**, *16*, 838.

[4] a) E. A. Phummer, A. Dijken, H. W. Hofstraat, L. De Cola, K. Brunner, *Adv. Funct. Mater.* **2005**, *15*, 281. b) J. D. Slinker, A. A. Gorodetsky, M. S. Lowry, J. Wang, S. Parker, R. Rohl, S. Bernhard, G. G. Malliaras, *J. Am. Chem. Soc.* **2004**, *126*, 2763. c) A. A. Gorodetsky, S. Parker, J. D. Slinker, D. A. Bernards, M. H. Wong, S. Flores-Torres, H. D. Abruña, G. G. Malliaras, *Appl. Phys. Lett.* **2004**, *84*, 807. d) J. D. Slinker, C. Y. Koh, G. G. Malliaras, M. S. Lowry, S. Bernhard, *Appl. Phys. Lett.* **2005**, *86*, 173 506.

[5] a) Z. Wang, A. R. McWilliams, C. E. B. Evans, X. Lu, S. Chung, M. A. Winnik, I. Manners, *Adv. Funct. Mater.* **2002**, *12*, 415. b) H. Y. Zhen, C. Y. Jiang, W. Yang, J. X. Jiang, F. Huang, Y. Cao, *Chem. Eur. J.* **2005**, *11*, 5007. c) X. Chen, J.-L. Liao, Y. Liang, M. O. Ahmed, H.-E. Tseng, S.-A. Chen, *J. Am. Chem. Soc.* **2003**, *125*, 636. d) A. J. Sandee, C. K. Williams, N. R. Evans, J. E. Davies, C. E. Boothby, A. Kohler, R. H. Friend, A. B. Holmes, *J. Am. Chem. Soc.* **2004**, *126*, 7041. e) J. X. Jiang, C. Y. Jiang, W. Yang, H. Y. Zhen, F. Huang, Y. Cao, *Macromolecules* **2005**, *38*, 4072. f) S. Tokito, M. Suzuki, F. Sato, M. Kamachi, K. Shirane, *Org. Electron.* **2003**, *4*, 105.

[6] a) S. T. Parker, J. D. Slinker, M. S. Lowry, M. P. Cox, S. Bernhard, G. G. Malliaras, *Chem. Mater.* **2005**, *17*, 3187. b) A. B. Tamayo, S. Garon, T. Sajoto, P. I. Djurovich, I. M. Tsyba, R. Bau, M. E. Thompson, *Inorg. Chem.* **2005**, *44*, 8723.

[7] a) X. Gong, M. R. Robinson, J. C. Ostrowski, D. Moses, G. C. Bazan, A. J. Heeger, *Adv. Mater.* **2002**, *14*, 581. b) X. Gong, J. C. Ostrowski, D. Moses, G. C. Bazan, A. J. Heeger, *Adv. Funct. Mater.* **2003**, *13*, 439. c) X. Gong, J. C. Ostrowski, G. C. Bazan, D. Moses, A. J. Heeger, M. S. Liu, A. K.-Y. Jen, *Adv. Mater.* **2003**, *15*, 45. d) F.-I. Wu, H.-J. Su, C.-F. Shu, L. Luo, W.-G. Diau, C.-H. Cheng, J.-P. Duan, G.-H. Lee, *J. Mater. Chem.* **2005**, *15*, 1035. e) X. Yang, D. Neher, D. Hertel, T. K. Däubler, *Adv. Mater.* **2004**, *16*, 161.

[8] a) J. Slinker, D. Bernards, P. L. Houston, H. D. Abruña, S. Bernhard, G. G. Malliaras, *Chem. Commun.* **2003**, 2392. b) S. Bernhard, X. Gao, G. G. Malliaras, H. D. Abruña, *Adv. Mater.* **2002**, *14*, 433. c) H. Rudmann, S. Shimada, M. F. Rubner, *J. Am. Chem. Soc.* **2002**, *124*, 4918. d) S. Bernhard, J. A. Barron, P. L. Houston, H. D. Abruña, J. L. Ruglovksy, X. Gao, G. G. Malliaras, *J. Am. Chem. Soc.* **2002**, *124*, 13 624. e) M. Buda, G. Kalyuzhny, A. J. Bard, *J. Am. Chem. Soc.* **2002**, *124*, 6090. f) H. Rudmann, S. Shimada, M. F. Rubner, *J. Am. Chem. Soc.* **2002**, *124*, 4918.

[9] R. Kannan, G. S. He, L. Yuan, F. Xu, P. N. Prasad, A. G. Dombroskie, B. A. Reinhardt, J. W. Baur, R. A. Waia, L.-S. Tan, *Chem. Mater.* **2001**, *13*, 1896.

[10] a) P. J. Low, B. A. J. Paterson, A. E. Goeta, D. S. Yufit, J. A. K. Howard, J. C. Cherryman, D. R. Tackley, B. Brown, *J. Mater. Chem.* **2004**, *14*, 2516. b) B. A. Reinhardt, L. L. Brott, S. J. Clarson, A. G. Dillard, J. C. Bhatt, R. Kannan, L. Yuan, G. S. He, P. N. Prasad, *Chem. Mater.* **1998**, *10*, 1863. c) J. W. Baur, M. D. Alexander, Jr., M. Banach, L. R. Denny, B. A. Reinhardt, R. A. Vaia, P. A. Fleitz, S. M. Kirkpatrick, *Chem. Mater.* **1999**, *11*, 2899. d) P. J. Low, M. A. Paterson, H. Puschmann, A. E. Goeta, J. A. K. Howard, C. Lambert, J. C. Cherryman, D. R. Tackley, S. Leeming, B. Brown, *Chem. Eur. J.* **2004**, *10*, 83.

[11] a) D. Neher, *Macromol. Rapid Commun.* **2001**, *22*, 1365. b) W.-Y. Wong, *Coord. Chem. Rev.* **2005**, *249*, 971.

[12] F. Neve, M. La Deda, A. Crispini, A. Bellusci, F. Puntoriero, S. Campagna, *Organometallics* **2004**, *23*, 5856.

[13] a) F. Neve, A. Crispini, S. Campagna, S. Serroni, *Inorg. Chem.* **1999**, *38*, 2250. b) S. Lamansky, P. Djurovich, D. Murphy, F. Abdel-Razzaq, R. Kwong, I. Tsyba, M. Bortz, R. Mui, R. Bau, M. E. Thompson, *Inorg. Chem.* **2001**, *40*, 1704. c) K. K. W. Lo, W. K. Hui, C. K. Chung, K. H. K. Tsang, D. C. M. Ng, N. Zhu, K. K. Cheung, *Coord. Chem. Rev.* **2005**, *249*, 1434.

[14] K. A. King, P. J. Spellane, R.-J. Watts, *J. Am. Chem. Soc.* **1985**, *107*, 1431.

[15] a) S. D. Cummings, R. Eisenberg, *J. Am. Chem. Soc.* **1996**, *118*, 1949. b) N. J. Demas, G. A. Crosby, *J. Am. Chem. Soc.* **1970**, *92*, 7262.

[16] M. Thelakkat, H.-W. Schmidt, *Adv. Mater.* **1998**, *10*, 219.

[17] A. Kraft, A. C. Grimsdale, A. B. Holmes, *Angew. Chem. Int. Ed.* **1998**, *37*, 402.

[18] a) K. M.-C. Wong, X. Zhu, L.-L. Hung, N. Zhu, V. W.-W. Yam, H.-S. Kwok, *Chem. Commun.* **2005**, 2906. b) J.-P. Duan, P.-P. Sun, C.-H. Cheng, *Adv. Mater.* **2003**, *15*, 224. c) C. H. Chen, J. Shi, C. W. Tang, *Macromol. Symp.* **1997**, *125*, 1.

[19] M. A. Baldo, C. Adachi, S. R. Forrest, *Phys. Rev. B* **2000**, *62*, 10 967.

[20] J. Kalinowski, W. Stampor, J. Mezyk, M. Cocchi, D. Virgili, V. Fattori, P. Di Marco, *Phys. Rev. B* **2002**, *66*, 235 321.

[21] M. J. Frisch, G. W. Trucks, H. B. Schlegel, G. E. Scuseria, M. A. Robb, J. R. Cheeseman, J. A. Montgomery, T. Vreven, Jr., K. N. Kudin, J. C. Burant, J. M. Millam, S. S. Iyengar, J. Tomasi, V. Barone, B. Mennucci, M. Cossi, G. Scalmani, N. Rega, G. A. Petersson, H. Nakatsuji, M. Hada, M. Ehara, K. Toyota, R. Fukuda, J. Hasegawa, M. Ishida, T. Nakajima, Y. Honda, O. Kitao, H. Nakai, M. Klene, X. Li, J. E. Knox, H. P. Hratchian, J. B. Cross, C. Adamo, J. Jaramillo, R. Gomperts, R. E. Stratmann, O. Yazyev, A. J. Austin, R. Cammi, C. Pomelli, J. W. Ochterski, P. Y. Ayala, K. Morokuma, G. A. Voth, P. Salvador, J. J. Dannenberg, V. G. Zakrzewski, S. Dapprich, A. D. Daniels, M. C. Strain, O. Farkas, D. K. Malick, A. D. Rabuck, K. Raghavachari, J. B. Foresman, J. V. Ortiz, Q. Cui, A. G. Baboul, S. Clifford, J. Cioslowski, B. B. Stefanov, G. Liu, A. Liashenko, P. Piskorz, I. Komaromi, R. L. Martin, D. J. Fox, T. Keith, M. A. Al-Laham, C. Y. Peng, A. Nanayakkara, M. Challacombe, P. M. W. Gill, B. Johnson, W. Chen, M. W. Wong, C. Gonzalez, J. A. Pople, *Gaussian 03*, revision B05, Gaussian, Inc., Pittsburgh, PA **2003**.

[22] a) W. R. Wadt, P. J. Hay, *J. Chem. Phys.* **1985**, *82*, 284. b) P. J. Hay, W. R. Wadt, *J. Chem. Phys.* **1985**, *82*, 299.

[23] G. Schaftenaar, *Molden v3.5*, CAOS/CAMM Center Nijmegen, Toernooiveld, Nijmegen, The Netherlands **1999**.